



UNIVERSITY OF LEEDS

This is a repository copy of *Deceleration of one-dimensional mixing by discontinuous mappings*.

White Rose Research Online URL for this paper:
<http://eprints.whiterose.ac.uk/123760/>

Version: Accepted Version

Article:

Kreczak, H, Sturman, R and Wilson, M orcid.org/0000-0002-1058-2003 (2017)
Deceleration of one-dimensional mixing by discontinuous mappings. *Physical Review E - Statistical, Nonlinear, and Soft Matter Physics*, 96 (5). 053112. ISSN 1539-3755

<https://doi.org/10.1103/PhysRevE.96.053112>

©2017 American Physical Society. This is an author produced version of a paper published in *Physical Review E*. Uploaded in accordance with the publisher's self-archiving policy.

Reuse

Unless indicated otherwise, fulltext items are protected by copyright with all rights reserved. The copyright exception in section 29 of the Copyright, Designs and Patents Act 1988 allows the making of a single copy solely for the purpose of non-commercial research or private study within the limits of fair dealing. The publisher or other rights-holder may allow further reproduction and re-use of this version - refer to the White Rose Research Online record for this item. Where records identify the publisher as the copyright holder, users can verify any specific terms of use on the publisher's website.

Takedown

If you consider content in White Rose Research Online to be in breach of UK law, please notify us by emailing eprints@whiterose.ac.uk including the URL of the record and the reason for the withdrawal request.



eprints@whiterose.ac.uk
<https://eprints.whiterose.ac.uk/>

DECELERATION OF ONE-DIMENSIONAL MIXING BY DISCONTINUOUS MAPPINGS

Hannah Kreczak ¹

*EPSRC CDT in Fluid Dynamics,
University of Leeds, LS2 9JT, United Kingdom*

Rob Sturman

*School of Mathematics,
University of Leeds, LS2 9JT, United Kingdom*

Mark C.T. Wilson

*School of Mechanical Engineering,
University of Leeds, LS2 9JT, United Kingdom*

Abstract

We present a computational study of a simple one-dimensional map with dynamics composed of stretching, permutations of equal sized cells, and diffusion. We observe that the combination of the aforementioned dynamics results in eigenmodes with long-time exponential decay rates. The decay rate of the eigenmodes is shown to be dependent on the choice of permutation and changes non-monotonically with the diffusion coefficient for many of the permutations. The global mixing rate of the map M in the limit of vanishing diffusivity approximates well the decay rates of the eigenmodes for small diffusivity, however this global mixing rate does not bound the rates for all values of the diffusion coefficient. This counter-intuitively predicts a deceleration in the asymptotic mixing rate with increasing diffusivity rate. The implication of the results on finite time mixing are discussed.

1 Introduction

Mixing processes occur in a variety of industrial and natural applications with large variation in time and length scales, however the outcomes of mixing are typically the same; there is a reduction of length scales, an increase in material interface and an approach to uniformity. Good mixing can be accomplished in fluids by the action of stretching and folding fluid elements (SF), either through a cascade to small scales via turbulent eddies or stirring protocols which consider chaotic trajectories in highly viscous fluids [1]. The kinematic behaviour of SF systems is captured well by the language of dynamical systems [2]. However, cutting and shuffling (CS), another mixing process, can create interface and increase segregation but does not involve material deformation. Discontinuous transformations such as cutting and shuffling have more subtle dynamics and are not well understood. Once there is a reduction in length scales by an advective process, molecular diffusion will blur any large gradients achieving uniformity of a scalar field in the long-time limit.

There are many instances in mechanical mixing in which discontinuities arise, although there is comparatively little understanding in their implication on mixing. Split-and-recombine micro-mixers adopt the action of cutting and shuffling to increase the number of lamellae between substances [3]. Sink-source flows, which may be configured to generate chaotic velocity profiles via pressure differences from fluid subtraction and reinjection, can introduce discontinuities by the closing and opening of valves during syringe reorientation [4, 5]. Streamline jumping, which occurs during reorientation, has been known to destroy dynamical features [6], or in the cut-dominated limit create

¹email address: mm10hek@leeds.ac.uk

pseudo-elliptic and pseudo-hyperbolic periodic points [7]. Additionally, underlying properties of the material may introduce discontinuities. High strain in polymeric, plastic or metallic material may cause slip deformations due to shear banding [8]. Granular materials also exhibit the mechanisms of both stretching and folding and cutting and shuffling. In tumbler flows, a flowing layer at the surface introduces shear-like behaviour while the bulk material undergoes solid body rotation. Piecewise isometries have been shown to capture the underlying structure in spherical tumbler flows [9, 10], with deviations in experimental models occurring due to the material passing through the flowing layer or diffusive-like effects from particle–particle interaction.

In applications of mixing, whether industrial or natural, it is a primary interest to quantify the rate of mixing to a certain condition. Molecular diffusion acting alone will cause a concentration field to tend to uniformity at an exponential rate, although this rate is generally very slow. Good stirring protocols can increase the rate to uniformity. In fully chaotic flows exponential stretching and compression of a fluid parcels produces an exponential rate in the reduction of length scales and increase in material interface. However, KAM surfaces and islands, boundaries surrounding fully chaotic domains, or parabolic points can contaminate this exponential mixing rate [11, 12]. The process of cutting and shuffling increases the number of interfaces linearly [13] and has been proven to be weak mixing in the asymptotic limit even in the absence of material stretching [14], but the mixing rate is at most polynomial [15]. Piecewise isometries on the unit interval or on a hemispherical shell have been shown to achieve good mixing even in finite time [16, 17, 18]. However, these mixing processes are unlikely to arise in isolation in real life applications.

There is an extensive literature studying the combination of stretching and folding from chaotic advection and diffusion, and the underlying mechanisms which drive the mixing rates. Uniform stretching with diffusion predicts an unrealistic super-exponential mixing rate, however non-uniformity in the underlying flow field produces exponential mixing rates overall. This rate is governed either through the mis-alignment of concentration field gradients with local stretching directions [19] or the global transport rate of the underlying flow field [20, 21, 22, 23]. The global regime leads to the emergence of “strange eigenmodes” [24], persistent patterns with a fixed exponential decay rate. The decay rate of the dominant eigenmode becomes independent of diffusivity in the zero-diffusivity limit [24, 20, 22].

Permutations of equal sized cells on the unit interval, a subset of interval exchange transformations (IET), have been shown to accelerate the asymptotic mixing rate of diffusion acting alone [25]. IETs with diffusion have been used as toy models to investigate mixing [26, 27] but there has been no investigation of the mixing rates of this larger parameter space. Bounds have been found on the mixing rates for permutations composed with expanding maps on the unit interval, with the conclusion that permutations do not improve the mixing rate and typically make it worse [28]. It is similarly reported for shears composed with a slip deformation that the combined mechanisms can slow the rate of mixing of material segregation [29].

There has however been no investigation into the composition of the three dynamics of SF, CS, and diffusion and the resulting mixing rates. We begin to address this here by studying a simple map on the unit interval of an idealised time-periodic and laminar fluid flow. In Sec 2 we construct the problem and introduce the hyperbolic and discontinuous maps. In Sec 3 we present the numerical results and in Sec 4 discuss the relationships to previously published results on expanding maps with permutations. In Sec 5 we consider the results in physical, finite time mixing and the implications of the results are discussed in Sec 6.

2 Formulation of the problem

2.1 Iterative Advection–Diffusion Map

We study the evolution of a passive scalar $c(\mathbf{x}, t)$ in a viscous fluid flow by the advection–diffusion equation

$$\partial_t c(\mathbf{x}, t) + u(\mathbf{x}, t) \cdot \nabla c(\mathbf{x}, t) = \kappa \nabla^2 c(\mathbf{x}, t), \quad (1)$$

over a domain Ω . The velocity field $u(\mathbf{x}, t)$ is taken to be incompressible, $\nabla \cdot u = 0$, and time periodic such that $u(\mathbf{x}, t + T) = u(\mathbf{x}, t)$. The diffusion coefficient κ is the inverse of the Peclet number $\kappa = Pe^{-1}$, a non-dimensional number representing the ratio of diffusive to advective timescales.

We simplify the evolution of the advection–diffusion equation by separating the processes of advection and diffusion in time. This iterative approach has been used previously to study mixing rates in one and two-dimensional chaotic maps [20, 21, 22]. First we evolve the scalar field according to (1) with $\kappa = 0$ for a time T . Since we are considering laminar time-periodic flows, we consider the advective step as a map $M : \Omega \rightarrow \Omega$ acting on fluid particles within the domain Ω as an iterative step in time $t \rightarrow t + T$ along the streamlines of the underlying flow field. Then the evolution of $c(\mathbf{x}, t) \rightarrow c(\mathbf{x}, t + T)$ can be represented by a linear operator acting on the space of functions $P_M : \mathcal{X} \rightarrow \mathcal{X}$, $c \in \mathcal{X}$. We consider the function class of piecewise smooth functions on the unit interval $\mathcal{X} = C_p^\infty[0, 1)$ as we are interested in studying transformations with discontinuities. The operator for the map is known as the Frobenius–Perron operator in the dynamics literature capturing the evolution of densities.

Following the advective time step, we then include diffusion by evolving the scalar field according to (1) with $u = 0$ via the operator $P_D : \mathcal{X} \rightarrow \mathcal{X}$, $P_D = \exp(t\kappa\nabla^2)$ for a time T . The operator for the full advective–diffusive time step is then considered as a composition of the operators $P = P_D \circ P_M$, such that $c^{(j+1)}(x) = (Pc^{(j)})(x)$ with $j = 0, 1, 2, \dots$ denoting the discrete steps. The operator P is linear due to the linearity of the advection–diffusion equation (1).

The eigenvalues λ_k of the operator P and their respective eigenfunctions v_k satisfy $Pv_k = \lambda_k v_k$ and the eigenvalues can be ordered according to their absolute values $|\lambda_1| \geq |\lambda_2| \geq \dots \geq 0$. The trivial eigenvalue $\lambda_1 = 1$ and the respective invariant eigenfunction is the mean field of the scalar \bar{c} . All other eigenvalues will have the value $|\lambda_k| < 1$ when the diffusion coefficient is non-zero.

We take a one-dimensional concentration field and the domain Ω to be the unit interval $\mathbb{T} = [0, 1)$ with periodic boundary conditions. Then the concentration field can be represented by the discrete Fourier expansion

$$c^{(j)}(x) = \sum_{n=-\infty}^{\infty} \hat{c}_n^{(j)} e^{2\pi i n x}.$$

The action of the operator P is then represented by the transfer of amplitude between the Fourier coefficients \hat{c}_n , given by

$$\hat{c}_n^{(j+1)} = \sum_{k=-\infty}^{\infty} d_{nm} M_{mk} \hat{c}_k^{(j)} \quad (2)$$

where the transfer matrix due to the advective map M is

$$M_{mk} = \int_0^1 e^{2\pi i m x - 2\pi i k M(x)} dx \quad (3)$$

and the diffusive step is defined via the transfer matrix

$$d_{nm} = \delta_{nm} \rho^{n^2}, \quad \rho = \exp(-4\pi^2 \kappa T). \quad (4)$$

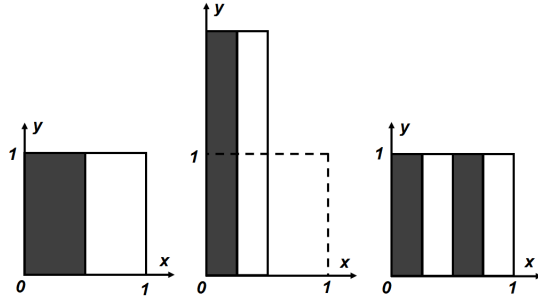


Figure 1: The action of the baker's map (5) is to contract the x direction, stretch the y direction and reassemble onto the unit torus. Taking a y independent initial condition, here $c(x, y) = \text{grey}$ for $x < 1/2$ and $c(x, y) = \text{white}$ for $x \geq 1/2$, reduces the baker's map to a one-dimensional map on the unit interval.

The time period for the diffusive step is normalised ($T = 1$) so that the effect of diffusion is parametrized by κ only.

2.2 Maps of interest

The two-dimensional incompressible baker's map is a paradigm example of a hyperbolic chaotic map which is mixing, given by the map

$$M_B(x, y) = \begin{cases} (x/2, 2y) & \text{for } y \in [0, 1/2) \\ ((x+1)/2, 2y-1) & \text{for } y \in [1/2, 1). \end{cases} \quad (5)$$

By considering a y independent initial condition, the baker's map reduces to a one-dimensional map which is one-to-two and represented acting on the concentration field by

$$c^{(j+1)}(x) = \begin{cases} c^{(j)}(2x) & \text{for } x \in [0, 1/2), \\ c^{(j)}(2(x-1)) & \text{for } x \in [1/2, 1). \end{cases}$$

Figure 1 depicts the action of the baker's map and its reduction to one-dimension.

We compose the baker's map with the simplest non-trivial piecewise isometry on the unit interval, a permutation of equal sized cells. The permutation map is applied by first dividing the unit interval into N equally sized intervals and numbering them according to their position within the interval. Consider a permutation $\sigma \in S_N$, where S_N is the group of all permutations on the set of symbols $\{1, 2, \dots, N\}$. Then the action of the map on a point $x \in [(l-1)/N, l/N)$ is given by

$$M_\sigma(x) = x + \frac{\sigma(l) - l}{N}. \quad (6)$$

The action on the concentration field is $c^{(j+1)}(x) = c^{(j)}(M_\sigma^{-1}(x))$. The permutations are represented in disjoint cycle notation, see [25] for example.

The composition of the maps M_B and M_σ will be denoted as a single map $\sigma \circ M_B$. The advantage of the chosen maps is that they are simple to implement in the transfer between Fourier coefficients. The advection-diffusion operator is represented as a single matrix by the product of matrices

$$\hat{c}_k^{(j+1)} = P_{nk} \hat{c}_n^{(j)}, \quad P_{nk} = d_{nm} M_{mk},$$

where the diffusive step matrix is taken as in (4) and the advective step

$$\begin{aligned} M_{mk} &= \int_0^1 e^{2\pi imx - 2\pi ik(\sigma \circ M_B(x))} dx \\ &= \frac{(1 - \omega^{(2k-m)})}{2\pi i(2k-m)} \sum_{\ell=1}^N \omega^{m\sigma(\ell) - 2k\ell} \end{aligned}$$

when $m \neq 2k$, with the primitive N th root of unity $\omega = e^{-2\pi i/N}$. When $m = 2k$,

$$M_{mk} = \frac{1}{N} \sum_{\ell=1}^N \omega^{m(\sigma(\ell) - \ell)}.$$

The computational process is then to truncate the Fourier modes to deal with finite matrices. Here we take $-K \leq k \leq K$, with $K = 1000$, which was sufficient for $\kappa \geq 10^{-6}$. Larger values of K showed no change in computational results. K can be increased accordingly for smaller values of κ .

We measure the decay of variance from the uniform distribution

$$\psi(j) = \int_0^1 |c^{(j)}(x) - \bar{c}|^2 dx = \sum_k |\hat{c}_k^{(j)}|^2 \quad (7)$$

to quantify the mixing rate. Subtracting the mean value \bar{c} as a constant, the rate of decay of variance is calculated in its approach to zero. A map which has good mixing will ensure that $c(x) \rightarrow \bar{c}$ quickly.

In the interest of the discussion here we only present results for $\sigma \in S_5$. For ease of discussion we define the rotation subgroup of S_N as the permutations σ which satisfy

$$\sigma(l) = l + m \pmod{N}$$

for $m \in \{0, 1, \dots, N-1\}$. Note that we have included the identity permutation in this group, which we denote S_N^R .

3 Numerical results

3.1 Initial transient

Figure 2 shows the decay of variance for a selection of permutations with $\kappa = 10^{-5}$ and the initial condition $c^{(0)}(x) = \cos(2\pi x)$. For a permutation $\sigma \in S_5^R$, the map reduces to $M(x) = 2x + m/N \pmod{1}$. Then $M_{mk} = \omega^{mk}$ for $m = 2k$ with $|\omega^{mk}| = 1$, and $M_{mk} = 0$ when $m \neq 2k$. Hence the resulting variance equation can be calculated analytically for all $\sigma \in S_N^R$ and for the initial condition $\cos(2\pi x)$ we have

$$\psi(j) = \psi(0) \cdot \exp\left(-\frac{32}{3}\pi^2 \kappa (4^j - 1)\right). \quad (8)$$

This result is the same as discussed in [21]. There is an exponential cascade to large wavenumbers, where the action of diffusion is more effective, leading to super-exponential decay in the variance. This is observed in the linear-log plot in Figure 3 for a representative permutation (12345).

For all other permutations $\sigma \in S_5 \setminus S_5^R$ the permutations create additional interface, transferring concentration to large wave numbers in the Fourier expansion immediately. These additional sharp

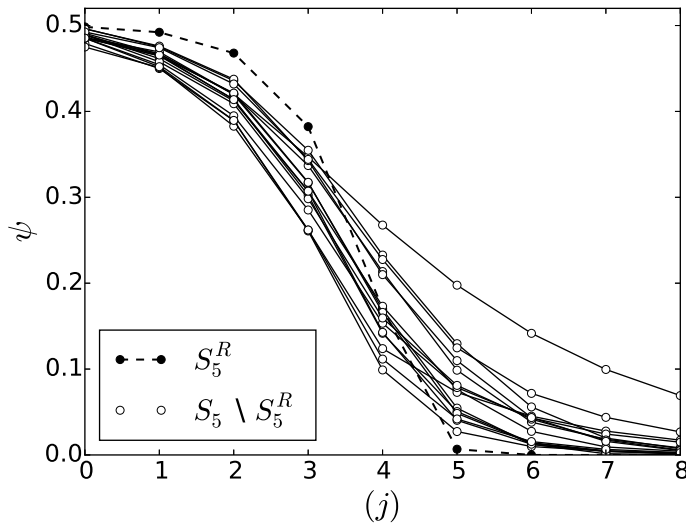


Figure 2: The initial stages of variance decay for representative permutations. Permutations which introduce new interface $S_5 \setminus S_5^R$ deplete the variance quicker than the identity of rotational permutations S_5^R in the initial 5 iterations. Diffusion coefficient is $\kappa = 10^{-5}$ with the initial condition $c^{(0)}(x) = \cos(2\pi x)$.

interfaces are not captured by stretching histories which implies that any local, Lagrangian arguments will break down in predicting the mixing rate of such a system. However, once there is a significant depletion of variance, the incompressible baker's map composed with $\sigma \in S_5^R$ depletes the variance quicker than any $\sigma \in S_5 \setminus S_5^R$.

3.2 Exponential Decay

For all $\sigma \in S_5 \setminus S_5^R$ the decay in concentration variance in the long-time limit is exponential. A sample of the variance profiles are seen in Figure 3, for the initial condition $c^{(0)}(x) = \cos(2\pi x)$ and $\kappa = 10^{-5}$. The variance profiles show significant variation in the exponential rates of decay for different permutations, also seen across a range of diffusivity coefficients.

The decay rates are predicted from the transfer matrices of the composed advection-diffusion iterative map P_{nk} . After a number of initial iterations the eigenfunctions v_k decay at the rate of their respective eigenvalues until the slowest decaying eigenfunction with the slowest decay rate, the second largest eigenvalue λ_2 , dominates the evolution of the concentration field. Hence the long-time exponential decay rate of the variance is given by $\psi(j) \sim |\lambda_2|^{2j}$, intuitive from (7). If $|\lambda_2| \sim 1$, then the decay rate of the dominant eigenfunction v_2 would be slow, while $|\lambda_2| \ll 1$ predicts a fast mixing rate.

The predicted decay rates from the eigenvalues are plotted as dashed lines in Figure 3 to show the precise agreement with the respective profiles. Oscillations arise due to the complex value of the eigenvalues and eigenfunctions [30]. The eigenfunctions are either static or spatially evolve on further applications of the operator P_{nk} . Figure 4 shows the emergence of a static eigenfunction for the permutation $\sigma = (34)$ after a number of initial iterations. Randomising the amplitudes of the

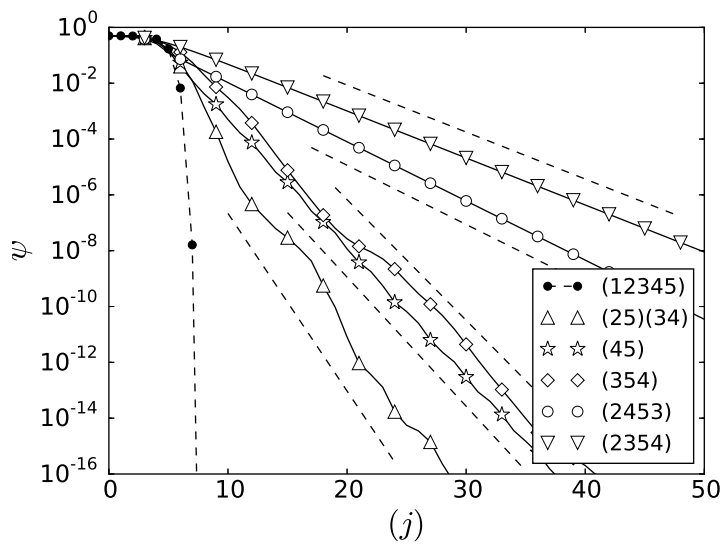


Figure 3: Variance decay profiles for representative permutations on linear-log axis. Dashed lines show the variance decay predicted by the second leading eigenvalues λ_2 . The diffusion coefficient is $\kappa = 10^{-5}$ with the initial condition $c^{(0)}(x) = \cos(2\pi x)$.

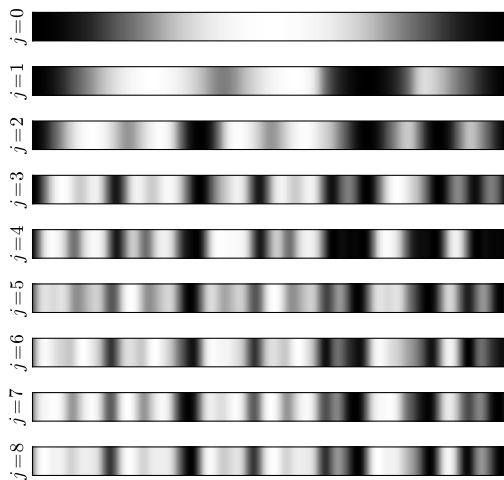


Figure 4: Image shows the first few iterations for the composed map with $\sigma \circ M_B$ with $\sigma = (34)$, $\kappa = 10^{-4}$ and the initial condition $c^{(0)}(x) = \cos(2\pi x)$. The colour scale is adjusted at each iteration to clearly show the persistent pattern emerging.

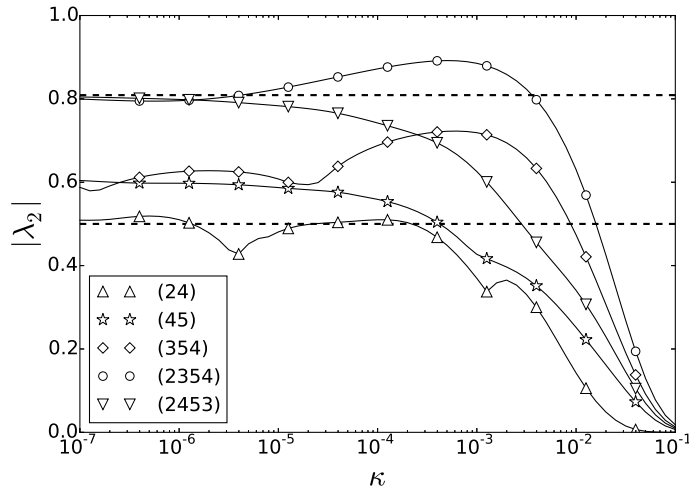


Figure 5: $|\lambda_2|$ is plotted against κ for a number of permutations. Convergence in the limit $\kappa \rightarrow 0$ occurs for some of the permutations while $|\lambda_2|$ changed non-monotonically for others. The dashed lines represent theoretical upper and lower bounds in the limit $\kappa = 0$. Symbols are used to distinguish the profiles and do not represent data points.

first four modes for the initial condition [30] results in the same eventual exponential decay rate. Hence we conclude that these are persistent patterns with decay rates irrespective of the initial condition, similar to those seen in chaotic advective systems with non-uniformity in the stretching rates of the flow field.

This is the well known global mechanism for mixing in smoothly deforming systems [20, 21, 22]. Dispersion between the Fourier modes occurs due to the permutation composition, comparable to the dispersion in non-uniform maps [21]. The decay rate is not governed by the local, Lagrangian behaviour since the stretching rates are the same almost everywhere, except for a countable number of discontinuities which form a set of zero measure. Non-uniformity arises in the rearrangement of striations by the interval exchange. Diffusive and reactive systems have been shown previously to be sensitive to striation arrangement [31]. However, unlike the strange eigenmodes of non-uniform smooth systems which align with regions of low stretching, the eigenmodes do not appear to correlate with physical characteristics of the underlying advective dynamics, such as periodic points or where the discontinuities are introduced.

According to the value of the second leading eigenvalues $|\lambda_2|$ for $\kappa = 10^{-3}, 10^{-4}, 10^{-5}$ and 10^{-6} , each permutation falls into one of 16 subgroups of S_5 . The subgroups consist of 5 or 10 permutations with $|\lambda_2|$ the same for all values of κ . The subgroups reflect rotations and reflections in the dynamics of the compositions on $\mathbb{T} = [0, 1)$ which is not intuitive from the permutations alone. For the rest of the paper we ignore $\sigma \in S_5^R$ and focus on permutations which have long time exponential decay of variance.

3.3 Effect of κ

A representative permutation from each of the 15 remaining subgroups was chosen and the second leading eigenvalue computed for many values of κ . Figure 5 shows several of the profiles which

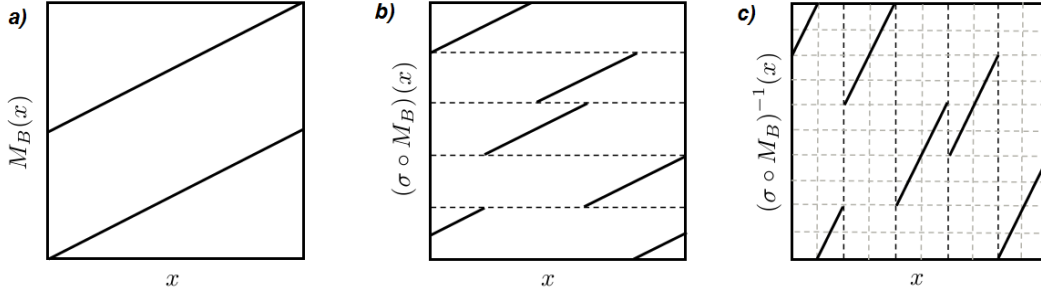


Figure 6: Graphical representations of a) one-dimensional approximation of the baker's map, the halving map, b) the halving map composed with the permutation $\sigma = (15243)$, denoted $(\sigma \circ M_B)$ and c) the pre-image map $(\sigma \circ M_B)^{-1}$ is shown with an appropriate Markov partition.

Table 1: For each of the subgroups, the absolute value of the second leading eigenvalues for low values of the diffusion coefficient, denoted $|\lambda_2^k|$, are computed. A comparison with τ , the mixing rate from the respective Markov transition matrices of the pre-image mapping $(\sigma \circ M_B)^{-1}$, shows good agreement.

| | | | | | | | | |
|-------------------------|--------|--------|--------|--------|----------|----------|--------|--------|
| | (45) | (34) | (345) | (354) | (35) | (23)(45) | (2354) | (2453) |
| $ \lambda_2^{10^{-7}} $ | 0.6042 | 0.6444 | 0.673 | 0.5878 | 0.6013 | 0.7493 | 0.7996 | 0.8046 |
| $ \lambda_2^{10^{-8}} $ | 0.6061 | 0.6518 | 0.6641 | 0.6235 | 0.5904 | 0.753 | 0.8075 | 0.807 |
| Markov τ | 0.5919 | 0.6624 | 0.6677 | 0.5755 | 0.5755 | 0.7564 | 0.809 | 0.809 |
| | (24) | (245) | (253) | (25) | (25)(34) | (13452) | (1345) | |
| $ \lambda_2^{10^{-7}} $ | 0.5751 | 0.8048 | 0.6443 | 0.6086 | 0.5089 | 0.8075 | 0.6156 | |
| $ \lambda_2^{10^{-8}} $ | 0.561 | 0.8072 | 0.6531 | 0.5926 | 0.4788 | 0.807 | 0.5808 | |
| Markov τ | 0.5 | 0.809 | 0.6624 | 0.5919 | 0.5 | 0.809 | 0.5 | |

highlight the behaviour seen. For some of the permutations there is convergence in the limit of $\kappa \rightarrow 0$ and the approach is monotonic with the diffusion coefficient, for example (2453) and (45). Convergence of mixing rates in the limit of small diffusivity is well observed numerically in non-uniform smooth chaotic deformations [24, 20, 32].

However non-monotonic profiles of the decay rates also occur with changing κ , for example (24), (354) and (2354), which has not been widely reported. If the subgroups were listed by the value of $|\lambda_2|$, then it is apparent from Figure 5 that the ordering would be dependent on the value of κ . [25] observed similar behaviour for permutations composed with diffusion, however non-monotonicity was not reported. Examples of maps in which non-monotonicity has been seen include an expanding map with three branches [33], and the non-uniform inverted baker's map with a no-flux boundary condition, where a power law relation had oscillatory non-monotonic behaviour [34]. Both maps contain points that are non-differentiable.

4 Mixing rates in the non-diffusive limit

In the absence of diffusion the variance of the concentration field would remain constant, however the advective operator P_M can be said to be ‘‘mixing’’ in the following sense [35]. Take sets $A, B \subset \Omega = [0, 1)$ and define the Lebesgue measure μ such that $A = [a, b)$, so that $\mu(A) = b - a$. Let $(\Omega, \mathcal{A}, \mu)$ be a normalized measure space where \mathcal{A} is the σ -algebra made up of all possible half-open subsets of the unit interval, and $M : \Omega \rightarrow \Omega$ a measure-preserving transformation. Then M is said to be *mixing* if

$$\lim_{n \rightarrow \infty} \mu(A \cap M^n(B)) = \mu(B)\mu(A) \text{ for all } A, B \subset \mathcal{A}. \quad (9)$$

For a map M which is not invertible we replace M^n with M^{-n} . This states that under the action of the map on the set A , we expect to find the same amount of A in any of the chosen intervals B . This can be re-formulated in functional form as the action of the map M on observable functions g and h via the *decay of correlations*

$$C_{g,h}(n) = \left| \int h(g \circ M^{-n})d\mu - \int gd\mu \int hd\mu \right|. \quad (10)$$

The rate at which $C_{g,h}(n) \rightarrow 0$ is of interest. Typically the observables g and h are representative of ‘a scalar field’. We refer to the following Lemma from [36]

Lemma 4.1 *For the Frobenius–Perron operator P which represents the map M , let \mathcal{X} be a class of real-valued functions preserved by P . Let $\sigma(P)$ denote the spectrum of P when considered as an operator on \mathcal{X} , and set $\tau = \sup\{|z| : z \in \sigma(P) \setminus \{1\}\}$. Then there is a constant $C < \infty$ such that $C_{gh}(N) \leq C\tau^N$ for all $N \geq 0$, if $g \in L^\infty$ and $h \in \mathcal{X}$*

Hence the decay of correlations, and thus the rate of mixing τ , is bounded by the second leading eigenvalue of the spectrum of P . It has previously been shown that the mixing rate given by the second leading eigenvalue in the small diffusivity limit tends to the second leading eigenvalue of the isolated spectrum for the advective operator P_M in smoothly deforming systems [32].

Thus, studying the spectrum of P_M will give an insight into the mixing rate of the composed map as $\kappa \rightarrow 0$. However, for $\kappa = 0$ the transfer matrix for the Fourier coefficients can not be feasibly truncated, thus it can not be found from the computational method already presented. The rate of mixing for the map when $\kappa = 0$ can be calculated from matrices defining the probability transition between Markov partitions for the map, the derivation of which closely follows methods developed for permutations composed with expanding maps and we briefly outline the results of [28].

An expanding map on the unit torus $[0, 1)$ is described as

$$f(x) = mx \pmod{1}, \quad m \in \mathbb{Z}, m \geq 2, \quad (11)$$

and the composition of expanding maps and permutations are denoted $\sigma \circ f$. The eigenvalues of Markov transition matrices representing the composed maps are related to the isolated spectrum of the composed map $\sigma \circ f$ through the use of Fredholm matrices. The absolute value of the second leading eigenvalue for the transition matrix is the value τ . It is proved that whenever N is not a multiple of m , the composition $\sigma \circ f$ acting on functions of bounded variation is always mixing, that is $\tau < 1$. A lower bound on τ is found to be $1/m$ and when $N > m$ and $\gcd(m, N) = 1$,

$$\tau \leq \tau_{max} = \frac{\sin(m\pi/N)}{m \sin(\pi/N)} \quad (12)$$

is a suitable upper bound.

The construction and results of [28] have a direct comparison with the current presented model. Consider the graphical representation of the system studied here; the halving map composed with a permutation, shown in Figure 6. We denote the pre-image $(\sigma \circ M_B)^{-1}$, which is also graphically presented. It is possible to construct a Markov partition on the pre-image map with $2 \times N$ elements of equal size $1/2N$ (N the number of cells in the permutation). It can easily be shown that an eigenvalue τ of the transformation $\sigma^{-1} \circ f$, is equivalent to the eigenvalue τ of $(\sigma \circ M_B)^{-1}$, where σ^{-1} denotes the inverse permutation of σ . This arises from the construction of the Markov transition matrices in the proof of the bounds from [28] (see the Appendix for details).

In reference to the definition of mixing given in (9), $(\sigma \circ M_B)^{-1}$ is not invertible and as such action of the map $\sigma \circ M_B$ is considered, which is precisely the evolution of striations we have studied here. Thus we compare the rates of mixing in the limit $\kappa \rightarrow 0$ to those predicted from the Markov transition matrices of $(\sigma \circ M_B)^{-1}$.

Table 1 compares τ for the pre-image $(\sigma \circ M_B)^{-1}$ with $|\lambda_2|$ of the respective diffusive transfer matrices in the limit of small diffusivity. The values show good agreement for many of the permutations, however this is not the case for all. Considering the permutations which are not in good agreement, profiles of $|\lambda_2|$ with κ for these permutations have non-monotonic behaviour with significant variation in the values of $|\lambda_2|$. It is not known whether the profiles will eventually converge or continue oscillating in the limit of small diffusivity but investigating smaller values of κ is computationally infeasible.

The lower and upper bounds on the value of τ for the model considered here are respectively

$$\tau_{min} = \frac{1}{2}, \quad \tau_{max} = \frac{\sin(2\pi/5)}{2 \sin(\pi/5)} \approx 0.809$$

and are plotted as dashed lines in Figure 5. τ_{max} and τ_{min} predict the slowest and fastest mixing rates of the operator $P_{\sigma \circ M_B}$ for $\sigma \in S_5$ respectively and seem to be reasonable bounds on the mixing rate when the diffusive rate is small. However, at large values of κ the upper bound does not agree as a bound on $|\lambda_2|$ due to the non-monotonicity of the profiles. For many of the permutations in the composed maps the second leading eigenvalue τ given by the Markov transition matrix is smaller than $|\lambda_2|$ for non-zero κ . Counter-intuitively this implies that the mixing rate is slower when the diffusive effect is large compared to the diffusivity in the zero-limit. To the authors' knowledge, although non-monotonicity has been reported previously, a slower mixing rate than the global transport rate in the zero diffusion limit has not.

Explaining the non-monotonicity is beyond the scope of this paper, although non-monotonicity in profiles of mixing rate with κ appear to persist when other hyperbolic maps on the unit interval are

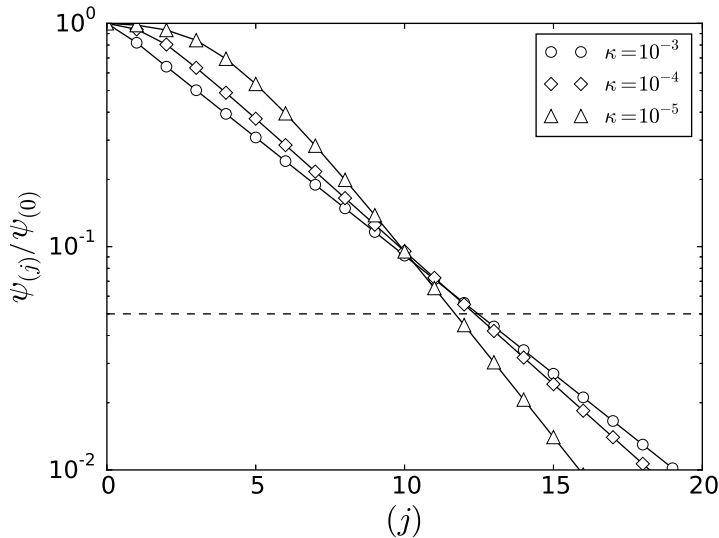


Figure 7: The variance $\psi(j)/\psi(0)$ is plotted for $\sigma \circ M_B$ with $\sigma = (2354)$, initial condition $c^{(0)}(x) = \cos(2\pi x)$, for three diffusivity values. Linear-log plot is used to better distinguish the iterates in which $\psi(j)/\psi(0)$ crosses the 95% threshold, represented by the dashed line. $\psi(j)/\psi(0)$ crosses the threshold at the earliest time when $\kappa = 10^{-5}$, the smallest value.

considered for the stretch and fold component, such as when the baker's map is the incompressible non-uniform baker's map [20] or inverted baker's map [37, 34]. The computational results of these maps composed with permutations are omitted for brevity.

5 Finite time mixing

The results of the paper thus far have been concerned with asymptotic mixing rates of the composed maps. However, mixing of concentration fields has several stages which contribute to the finite time mixing and in practical situations one would want to consider the time need to mix to a desired condition. We consider the finite mixing rate by first returning to means of quantify mixing under the action of advection and diffusion. We introduce the L^∞ and L^q norms;

$$\begin{aligned} L_t^\infty &= \|c(x, t) - \bar{c}\|_\infty \\ &= \inf\{M : |c(x, t) - \bar{c}| \leq M \text{ a.e. } x \in [0, 1]\} \end{aligned}$$

and

$$L_t^q = \|c(x, t) - \bar{c}\|_q = \left(\int_0^1 |c(x, t) - \bar{c}|^q dx \right)^{1/q}.$$

In this paper we have already considered the variance which is defined $\|c(x, t) - \bar{c}\|_2^2$, the square of the L^2 norm. Which norm to consider depends on the application and desired result. Note that taking $0 < q' \leq q$ then $\|\cdot\|_q \leq \|\cdot\|_{q'} \leq \|\cdot\|_\infty$. Similar to a previous study [25], we consider the time needed for a desired norm to come within an arbitrary condition, say 5% of uniform, which is

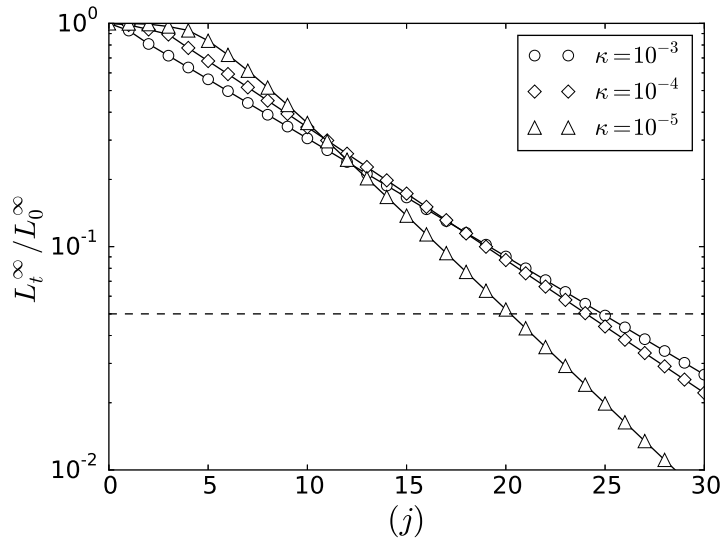


Figure 8: L_t^∞/L_0^∞ norm is plotted for $\sigma \circ M_B$ with $\sigma = (2354)$, initial condition $c^{(0)}(x) = \cos(2\pi x)$, for three diffusivity values. Linear-log plot is used to better distinguish the iterates in which L_t^∞/L_0^∞ crosses the 95% threshold, represented by the dashed line. Similar to the variance, L_t^∞/L_0^∞ crosses the threshold at the earliest time when $\kappa = 10^{-5}$, the smallest value.

referred to as the *time to 95% mixing*, t_{95} . It is defined to be the smallest $t_{95} = t > 0$ such that

$$\|c(x, t) - \bar{c}\|_q / \|c(x, 0) - \bar{c}\|_q \leq 0.05 \quad (13)$$

where q denotes the L^q norm. We numerically investigate the number of iterates needed to satisfy this requirement for the L^∞ norm and ψ .

In the initial stages of advection and diffusion, when the effect of diffusivity is small, an L^q norm will remain constant for some time until the gradients or lengthscales in the concentration field are on the order of the Batchelor lengthscale $\sqrt{\kappa/\lambda_{ls}}$, the balance between diffusive rate and local strain rate λ_{ls} . For smoothly deforming chaotic flows, in the limit of small diffusivity the exponential mixing rate becomes independent of the diffusivity coefficient in the limit of small diffusivity, thus the main consequence of decreasing the effect of diffusivity is to extend the initial transient where a measured norm is close to constant. Once the Batchelor scale is reached there is significant decay, however this initial stage is weakly dependent on diffusivity, on the order of $\log(\kappa)$ [21, 38].

As an example, we take the permutation $\sigma = (2354)$, which has a slower asymptotic mixing rate at non-zero κ than the upper bound on the zero-diffusivity mixing rate. The initial condition is taken to be $\cos(2\pi x)$. Figure 7 plots the variance decay rates for three different values of κ . The renormalised variance of $c^{(j)}(x)$ for the larger values of $\kappa = 10^{-3}, 10^{-4}$ achieves the 95% mixed state after the smallest value $\kappa = 10^{-5}$, although the difference is approximately 1 iteration. However, for the L^∞ norm in Figure 8, the condition for the larger diffusivity rates is reached approximately 5 iterations later. This example illustrates that the counter-intuitive deceleration with diffusivity rate κ could have a significant effect on the time to achieve a practical mixing condition. In applications of fluid mixing devices this would equate to 5 additional stirring periods or channel segments to achieve the desired result, which could be overlooked if approximating mixing time from advective

properties only and thus the correct mixing criteria not achieved in the predicted time.

6 Discussion

We have presented a one-dimensional model which captures a mixture of stretching and discontinuous advective dynamics with a diffusive step. In the initial transient the additional discontinuities speed up the decay of variance over the chaotic advection alone. However once the Batchelor scale is reached and variance begins to deplete, a phase of exponential decay begins due to the non-uniformity caused by the permutation of striation arrangement. Lagrangian arguments fail to explain the varying decay rates across the range of permutations since stretching rates are the same almost everywhere, except where they are undefined on the discontinuities which form a set of measure zero. The mechanism for the emergence of an exponential asymptotic mixing rate is global and in the limit $\kappa \rightarrow 0$ the mixing rate is well approximated by the global transport rate predicted from the Markov partitions of the pre-image map.

However, this approach to the mixing rate in the zero diffusivity limit is non-monotonic in many cases which is counter intuitive. Although non-monotonicity has been observed in one-dimensional maps before [34] [33], here a slower mixing rate than the global mixing rate is predicted for large values of the diffusivity coefficient, which has not been previously reported. However, all maps in which non-monotonicity with diffusion has been reported have a common property in that they contain points which are non-differentiable. We hypothesise that this deceleration with diffusion is a feature of non-continuous mappings in which discontinuous transformations are a subset. In the dynamical systems and ergodic theory literature there is large interest in finding global mixing rates of advective maps and bounds on these mixing rates, but these computational results suggest that in studying fluid mixing systems in which there is a mixture of stretching and cutting and shuffling, diffusion may have to be taken into account for accurate mixing rate predictions and comparisons across mixing protocols. The significance in this observation is shown to effect mixing rates in finite time considerations to achieve physical mixing conditions, chosen arbitrarily here to be a 95% mixed state.

The present study could be extended to a larger collection of interval exchange transformations with finite order, however the similarities of the mixing rates for small diffusivity to the rates τ when $\kappa = 0$ implies that the conclusions of [28] predict well the asymptotic mixing rates and it is unlikely that adding diffusion would not highlight anything of further interest than already discussed herein. The model is highly idealised in relation to real fluid mixing problems. The one-dimensional reduction of the baker's map leads to a striation arrangement which are all perfectly aligned with the stable manifolds and notably, the discontinuities are also aligned with the stable manifolds. One possible extension would be to study the same phenomena in a two-dimensional system where one of these idealisations is not present.

Acknowledgements

HK would like to thank Jean-Luc Thiffeault for helpful discussions while visiting the University of Madison–Wisconsin, USA. HK is funded by EPSRC via grant EP/L01615X/1.

Appendix

In this appendix we briefly discuss the construction of the Markov partitions and highlight the required results of [28] to find the mixing rates for $\sigma \circ M_B$ when $\kappa = 0$.

The Markov partitions for the composition map $\sigma \circ f$, where $\sigma \in S_N$ and f as defined in (11), are constructed as follows. Define P_k by $\{0, 1, \dots, k-1\}$ and number the associated rows and columns in the transition matrices from 0. $A(m, N)$ and $B(m, N)$ are defined to be the state transition matrices for the expanding map f with respect to P_N and P_{Nm} respectively and are found via

$$A(m, N)_{ij} = \begin{cases} 1 & \text{if } j = mi + d \bmod N, \ 0 \leq d \leq m-1, \\ 0 & \text{otherwise,} \end{cases}$$

and

$$B(m, N)_{ij} = \begin{cases} 1 & \text{if } j = mi + d \bmod Nm, \ 0 \leq d \leq m-1, \\ 0 & \text{otherwise.} \end{cases}$$

The state transition matrices for $\sigma \circ f$ are then obtained by permuting the columns of $A(m, N)$ and $B(m, N)$. $P(\sigma)$ is defined as

$$P(\sigma) = \begin{cases} 1 & \text{if } j = \sigma(i), \\ 0 & \text{otherwise,} \end{cases}$$

and let $Q(\sigma)$ be the $Nm \times Nm$ matrix obtained by replacing each entry 1 in $P(\sigma)$ by an $m \times m$ identity matrix, and each 0 entry by a $m \times m$ zero matrix. Then the state transition matrices for $\sigma \circ f$ w.r.t P_N and P_{Nm} are $A(m, N)P(\sigma)$ and $B(m, N)Q(\sigma)$. It is proved in Lemma 4.2.1. [28] that the eigenvalues of $A(m, N)P(\sigma)$ and $B(m, N)Q(\sigma)$ are the same.

When considering the state transition matrices of the pre-image $(\sigma \circ M_B)^{-1}$, the same construction can be followed in which the rows are permuted instead of the columns; $P(\sigma)A(m, N)$ and $Q(\sigma)B(m, N)$. By the same arguments in Lemma 4.2.1 [28], a vector space can be constructed which proves that the second leading eigenvalues of $P(\sigma)A(m, N)$ and $Q(\sigma)B(m, N)$ are also equivalent.

Finally, note that $P(\sigma)A(m, N)$ is the matrix obtained from $A(m, N)P(\sigma^{-1})$ and if $\tilde{\tau}$ is an eigenvalue of $P(\sigma)A(m, N)$, then $\tau = \tilde{\tau}/m$, hence for every σ , $\tau_{\sigma^{-1} \circ f} = \tau_{(\sigma \circ M_B)^{-1}}$.

References

- [1] H. Aref, "Stirring by chaotic advection," *J. Fluid Mech*, vol. 143, pp. 1–21, 1984.
- [2] J. M. Ottino, *The kinematics of mixing: stretching, chaos, and transport*. Cambridge university press, 1989.
- [3] D. Hobbs and F. Muzzio, "The kenics static mixer: a three-dimensional chaotic flow," *Chem. Eng. J.*, vol. 67, no. 3, pp. 153–166, 1997.
- [4] S. W. Jones and H. Aref, "Chaotic advection in pulsed source–sink systems," *Phys. Fluids*, vol. 31, no. 3, pp. 469–485, 1988.
- [5] J.-M. Hertzsch, R. Sturman, and S. Wiggins, "Dna microarrays: design principles for maximizing ergodic, chaotic mixing," *Small*, vol. 3, no. 2, pp. 202–218, 2007.
- [6] D. R. Lester, G. Metcalfe, M. G. Trefry, A. Ord, B. Hobbs, and M. Rudman, "Lagrangian topology of a periodically reoriented potential flow: Symmetry, optimization, and mixing," *Phys. Rev. E*, vol. 80, no. 3, p. 036208, 2009.

- [7] L. D. Smith, M. Rudman, D. R. Lester, and G. Metcalfe, “Mixing of discontinuously deforming media,” *Chaos*, vol. 26, no. 2, p. 023113, 2016.
- [8] D. V. Louzguine-Luzgin, L. V. Louzguina-Luzgina, and A. Y. Churyumov, “Mechanical properties and deformation behavior of bulk metallic glasses,” *Metals*, vol. 3, no. 1, pp. 1–22, 2012.
- [9] R. Sturman, S. Meier, J. Ottino, and S. Wiggins, “Linked twist map formalism in two and three dimensions applied to mixing in tumbled granular flows,” *J. Fluid Mech.*, vol. 602, pp. 129–174, 2008.
- [10] G. Juarez, I. C. Christov, J. M. Ottino, and R. M. Lueptow, “Mixing by cutting and shuffling 3d granular flow in spherical tumblers,” *Chem. Eng. Sci.*, vol. 73, pp. 195–207, 2012.
- [11] E. Gouillart, O. Dauchot, B. Dubrulle, S. Roux, and J.-L. Thiffeault, “Slow decay of concentration variance due to no-slip walls in chaotic mixing,” *Phys. Rev. E*, vol. 78, no. 2, p. 026211, 2008.
- [12] J. Springham and R. Sturman, “Polynomial decay of correlations in linked-twist maps,” *Ergodic Theory Dyn. Syst.*, vol. 34, no. 05, pp. 1724–1746, 2014.
- [13] C. F. Novak, “Discontinuity-growth of interval-exchange maps,” vol. 3, 07 2009.
- [14] A. Avila and G. Forni, “Weak mixing for interval exchange transformations and translation flows,” *Ann. Math.*, pp. 637–664, 2007.
- [15] A. Katok, “Interval exchange transformations and some special flows are not mixing,” *Israel J. Math.*, vol. 35, no. 4, pp. 301–310, 1980.
- [16] M. K. Krotter, I. C. Christov, J. M. Ottino, and R. M. Lueptow, “Cutting and shuffling a line segment: Mixing by interval exchange transformations,” *Int. J. Bifurc. Chaos*, vol. 22, no. 12, p. 1230041, 2012.
- [17] M. Yu, P. B. Umbanhowar, J. M. Ottino, and R. M. Lueptow, “Cutting and shuffling of a line segment: Effect of variation in cut location,” *Int. J. Bifurc. Chaos*, vol. 26, no. 14, p. 1630038, 2016.
- [18] P. P. Park, P. B. Umbanhowar, J. M. Ottino, and R. M. Lueptow, “Mixing with piecewise isometries on a hemispherical shell,” *Chaos*, vol. 26, no. 7, p. 073115, 2016.
- [19] T. M. Antonsen Jr, Z. Fan, E. Ott, and E. Garcia-Lopez, “The role of chaotic orbits in the determination of power spectra of passive scalars,” *Phys. Fluids*, vol. 8, no. 11, pp. 3094–3104, 1996.
- [20] D. R. Fereday, P. H. Haynes, A. Wonhas, and J. C. Vassilicos, “Scalar variance decay in chaotic advection and batchelor-regime turbulence,” *Phys. Rev. E*, vol. 65, no. 3, p. 035301, 2002.
- [21] A. Wonhas and J. C. Vassilicos, “Mixing in fully chaotic flows,” *Phys. Rev. E*, vol. 66, no. 5, p. 051205, 2002.
- [22] J.-L. Thiffeault and S. Childress, “Chaotic mixing in a torus map,” *Chaos*, vol. 13, no. 2, pp. 502–507, 2003.
- [23] A. Pikovsky and O. Popovych, “Persistent patterns in deterministic mixing flows,” *Europhys. Lett.*, vol. 61, no. 5, p. 625–631, 2003.
- [24] R. Pierrehumbert, “Tracer microstructure in the large-eddy dominated regime,” *Chaos Solitons Fractals*, vol. 4, no. 6, pp. 1091–1110, 1994.
- [25] P. Ashwin, M. Nicol, and N. Kirkby, “Acceleration of one-dimensional mixing by discontinuous mappings,” *Physica A*, vol. 310, no. 3, pp. 347–363, 2002.
- [26] G. Froyland, C. González-Tokman, and T. M. Watson, “Optimal mixing enhancement by local perturbation,” *SIAM Rev.*, vol. 58, no. 3, pp. 494–513, 2016.
- [27] R. Sturman, “The role of discontinuities in mixing,” *Adv. Appl. Mech.*, vol. 45, no. 51, p. 2012, 2012.
- [28] N. Byott, M. Holland, and Y. Zhang, “On the mixing properties of piecewise expanding maps under composition with permutations,” *Discrete Contin. Dyn. Syst.*, vol. 33, no. 8, p. 3365–3390, 2013.
- [29] L. D. Smith, M. Rudman, D. R. Lester, and G. Metcalfe, “Impact of discontinuous deformation upon the rate of chaotic mixing,” *Phys. Rev. E*, vol. 95, no. 2, p. 022213, 2017.

- [30] V. Toussaint, P. Carrière, and F. Raynal, “A numerical eulerian approach to mixing by chaotic advection,” *Phys. Fluids*, vol. 7, no. 11, pp. 2587–2600, 1995.
- [31] M. Clifford, S. Cox, and E. Roberts, “Reaction and diffusion in a lamellar structure: the effect of the lamellar arrangement upon yield,” *Physica A*, vol. 262, no. 3, pp. 294–306, 1999.
- [32] P. Haynes and J. Vanneste, “What controls the decay of passive scalars in smooth flows?,” *Phys. Fluids*, vol. 17, no. 9, p. 097103, 2005.
- [33] B. Eckhardt, E. Hascoët, and W. Braun, “Passive fields and particles in chaotic flows,” in *IUTAM Symposium on Nonlinear Stochastic Dynamics*, pp. 415–424, Springer, 2003.
- [34] A. D. Gilbert, “Advection fields in maps—iii. passive scalar decay in baker’s maps,” *Dynam. Syst.*, vol. 21, no. 1, pp. 25–71, 2006.
- [35] R. Sturman, J. M. Ottino, and S. Wiggins, *The mathematical foundations of mixing: the linked twist map as a paradigm in applications: micro to macro, fluids to solids*. Cambridge University Press, 2006.
- [36] G. Froyland, *Extracting dynamical behavior via Markov models*, p. 281. Berlin: Birkhäuser Verlag AG, 2001.
- [37] E. Gouillart, N. Kuncio, O. Dauchot, B. Dubrulle, S. Roux, and J.-L. Thiffeault, “Walls inhibit chaotic mixing,” *Phys. Rev. Lett.*, vol. 99, no. 11, p. 114501, 2007.
- [38] J.-L. Thiffeault, *Scalar decay in chaotic mixing*, pp. 3–36. Springer, 2008.